Supplementary material

Moderate L-lactate administration suppresses adipose tissue macrophage M1 polarization to alleviate obesity-associated insulin resistance

Authors: Hao Cai, Xin Wang, Zhixin Zhang, Juan Chen, Fangbin Wang, Lu Wang, Jian Liu*

* **Corresponding author:** Jian Liu

E-mail: liujian509@hfut.edu.cn

The Supplemental material includes:

Fig. S1-10 (included in this file)

Table. S1-2 (included in this file)

Figure S1. The insulin signaling cascades in the liver and skeletal muscle. The 6-week-old male mice were divided into four groups, including LS, LL, HS, and HL groups. **A** The GLUT2 translocation in the liver and quantification of plasma membrane GLUT2 to total GLUT2; Immunoblots for phosphorylation level of AKT in the liver. **B** The GLUT4 translocation in the skeletal muscle and quantification of plasma membrane GLUT4 to total GLUT4; Immunoblots for phosphorylation level of AKT in the skeletal muscle. Data are presented as means ± SD of 8 mice per group, one-way ANOVA with Mann-Whitney test; *$p < 0.05$, **$p < 0.01$, ***$p < 0.001$. LS, LFD-saline (i.p.); LL, LFD-lactate (i.p.); HS, HFD-saline (i.p.); HL, HFD-lactate (i.p.); PM, Plasma membrane.

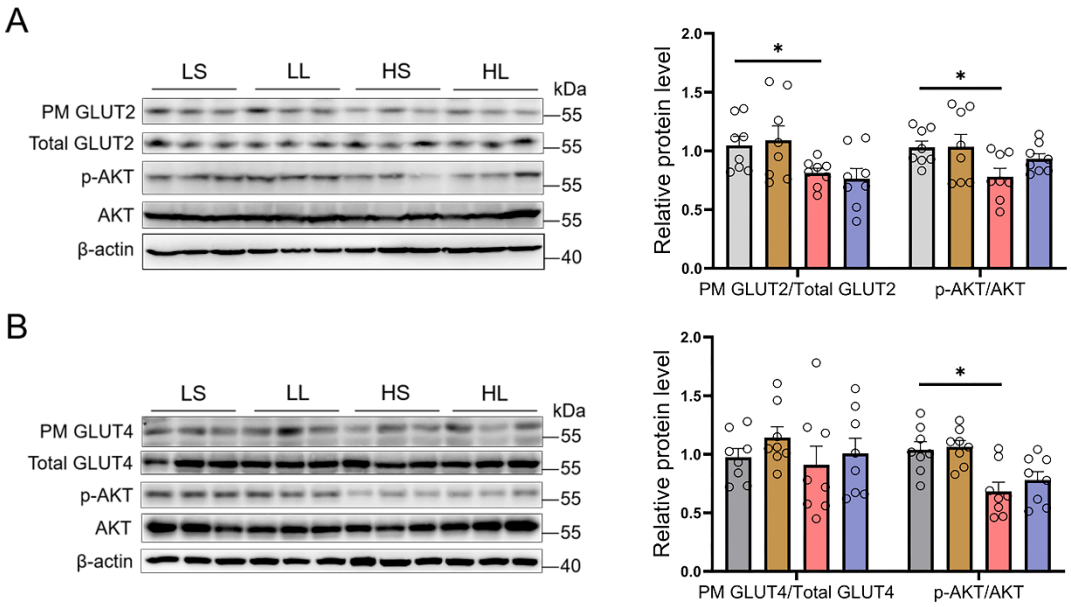

Figure S2. Moderate L-lactate administration did not lead to the development of hyperlactatemia or lactic acidosis. The 6-week-old male mice were divided into four groups, including LS, LL, HS, and HL groups. **A** The serum pH value. **B** Food intake. **C** Energy intake. **D** Liver weight. **E** Spleen weight. **F-G** The serum ALT **(F)** and AST **(G)**. **H** The H&E staining of liver and spleen; scale bar, 100 μm. Data are presented as means ± SD of 8 mice per group, one-way ANOVA with Mann-Whitney test; *$p < 0.05$, **$p < 0.01$, ***$p < 0.001$. LS, LFD-saline (i.p.); LL, LFD-lactate (i.p.); HS, HFD-saline (i.p.); HL, HFD-lactate (i.p.); ALT, Alanine transaminase; AST, Aspartate aminotransferase.

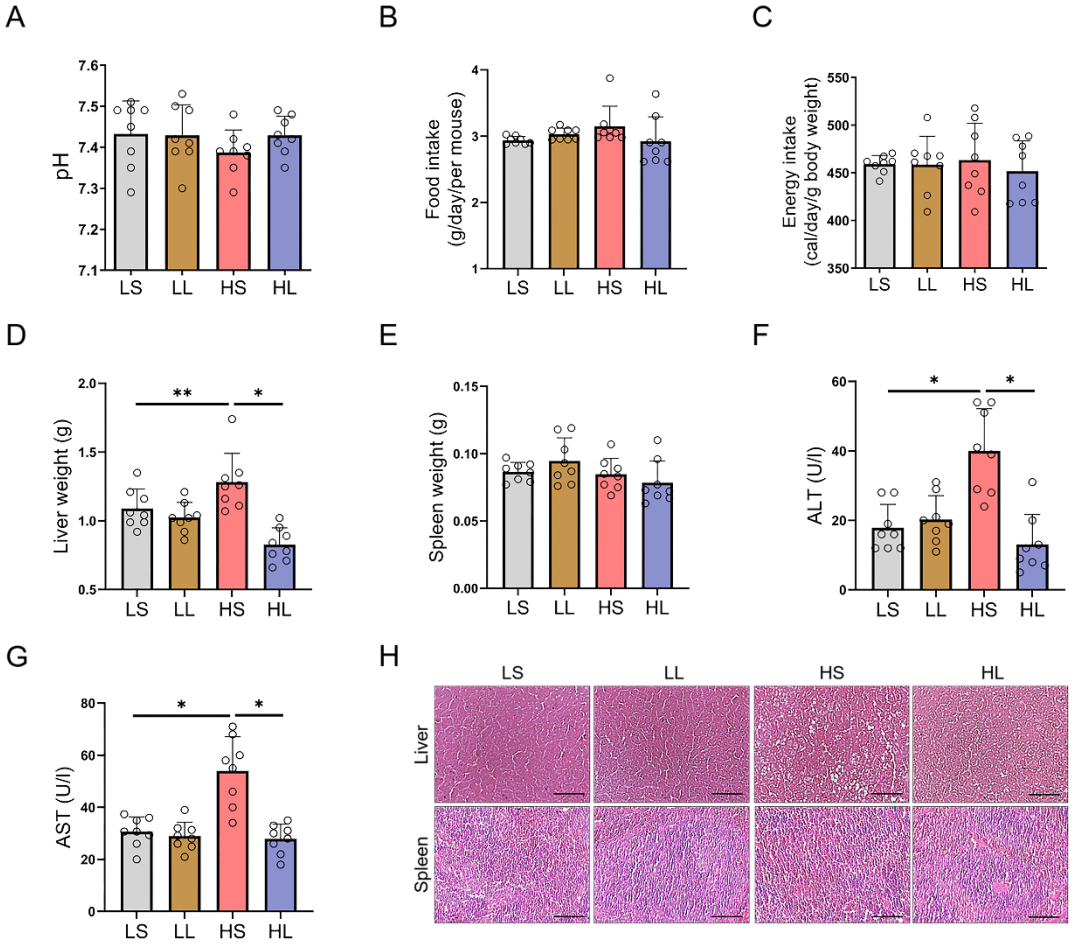

Figure S3. The effects of moderate L-lactate administration on energy expenditure in LFD and HFD-fed mice. At the age of 18 weeks, the metabolic capability in mice from four groups was measured. **A-B** VO_2 **(A)** and VCO_2 **(B)** per g body weight were detected without L-lactate injection during a 24-hour light-dark cycle. **C-D** VO_2 **(C)** and VCO_2 **(D)** per mouse were detected without L-lactate injection during a 24-h light-dark cycle. **E-F** VO_2 **(E)** and VCO_2 **(F)** per g body weight were detected during a 24-hour light-dark cycle and 400mg/kg L-lactate was injected at 9 a.m. and 6 p.m. Data are presented as means ± SD of 8 mice per group, one-way ANOVA with Mann-Whitney test. *$p < 0.05$, **$p < 0.01$, ***$p < 0.001$ compared with HS group; #$p < 0.05$, ##$p < 0.01$, ###$p < 0.001$, LL group was compared with LS group. LS, LFD-saline (i.p.); LL, LFD-lactate (i.p.); HS, HFD-saline (i.p.); HL, HFD-lactate (i.p.); VO_2, Oxygen consumption; VCO_2, Carbon dioxide production.

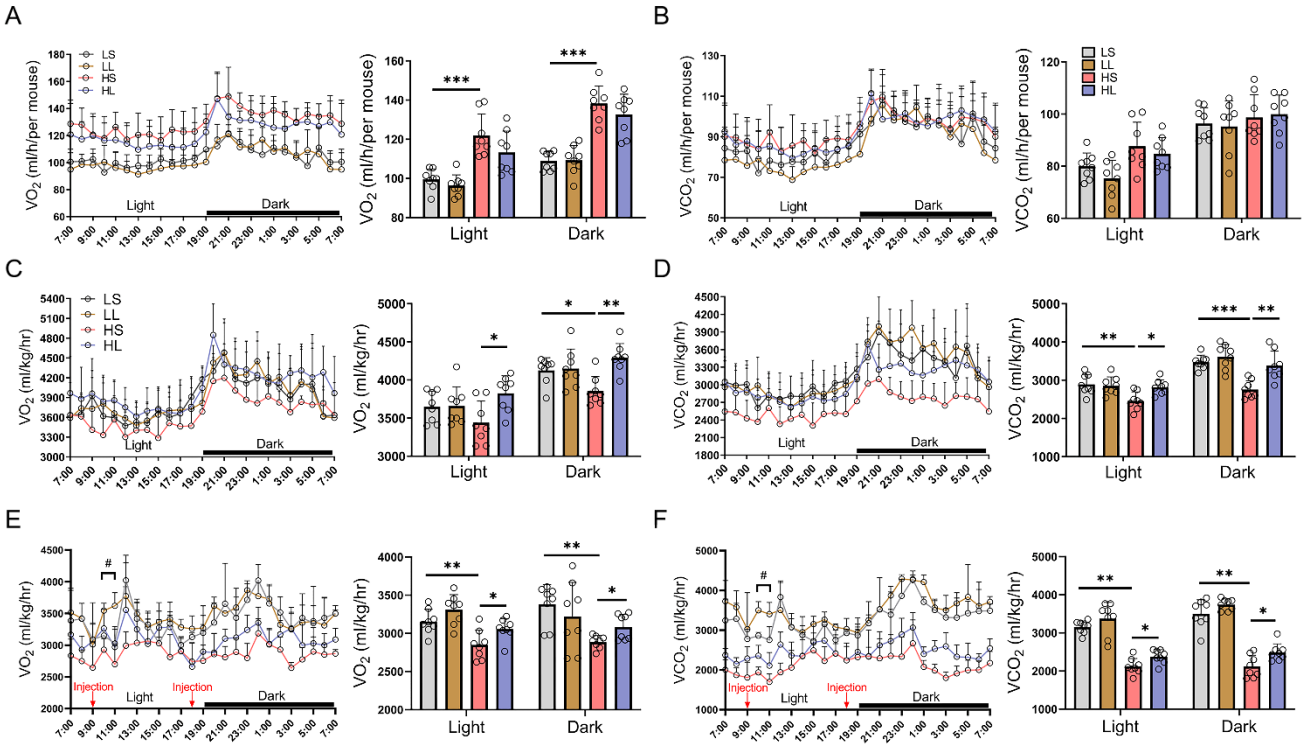

Figure S4. The fatty acid oxidation and glucose catabolism in the liver and skeletal muscle. The 6-week-old male mice were divided into four groups, including LS, LL, HS, and HL groups. **A-B** The relative genes of fatty acid oxidation and glucose catabolism in the liver **(A)** and skeletal muscle **(B)**. Data are presented as means ± SD of 8 mice per group, one-way ANOVA with Mann-Whitney test; *p < 0.05, **p < 0.01, ***p < 0.001. LS, LFD-saline (i.p.); LL, LFD-lactate (i.p.); HS, HFD-saline (i.p.); HL, HFD-lactate (i.p.).

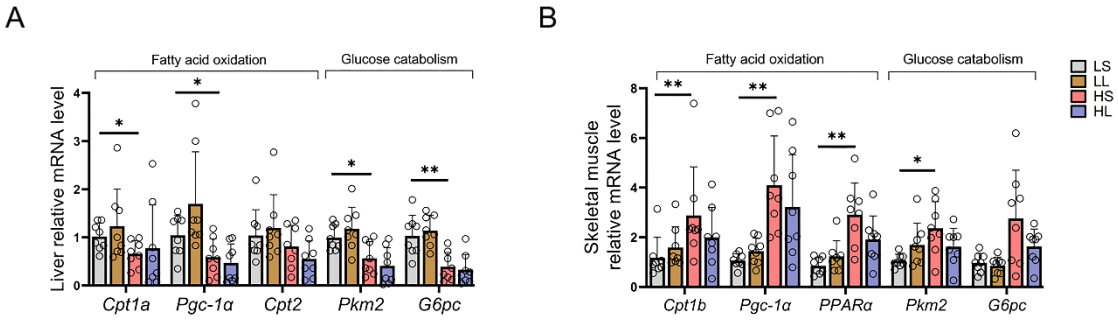

Figure S5. The expression of MCT1 in ATMs and BMDMs after inflammatory stimulation. The 6-week-old male mice were divided into four groups, including LS, LL, HS, and HL groups. **A** The mRNA level of *MCT1* in EATs. **B** The mRNA level of *MCT1* in ATMs from EATs. BMDMs were treated with vehicle or L-lactate (5 mM or 10 mM), and then LPS was added. **C** The mRNA level of *MCT1* in BMDMs. Data are presented as means ± SD of 8 mice per group in vivo, 4 parallel cell samples per group in ATMs and 6 parallel cell samples per group in BMDMs, one-way ANOVA with Mann-Whitney test for mice and two-tailed Student's t-test for cell samples; *$p <$ 0.05, **$p < 0.01$, ***$p < 0.001$. LS, LFD-saline (i.p.); LL, LFD-lactate (i.p.); HS, HFD-saline (i.p.); HL, HFD-lactate (i.p.); Lac, Lactate; EAT, Epididymal adipose tissue; ATM, Adipose tissue macrophage.

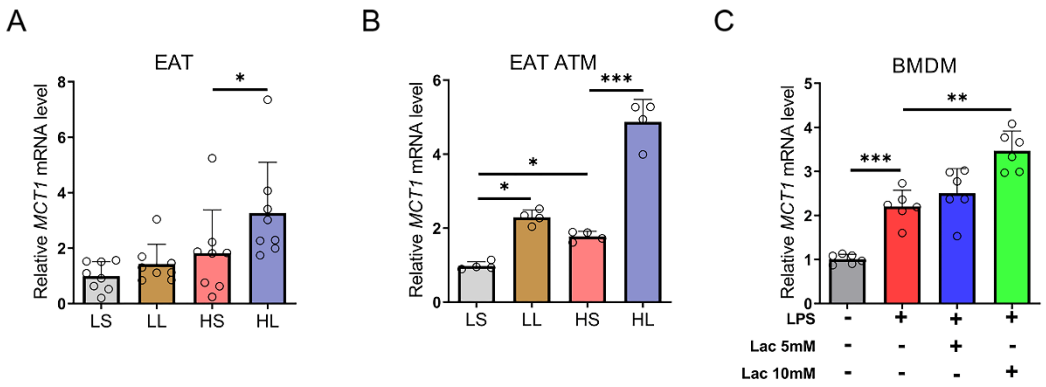

Figure S6. The expression of GPR132 in adipocytes and SVFs. A The mRNA level of *GPR132* in adipocytes and SVFs from EATs in HFD-fed mice. **B** The mRNA level of *GPR132* in primary adipocytes after L-lactate treatment. **C** The mRNA level of *GPR132* in SVFs after L-lactate treatment. Data are presented as means ± SD of 4 parallel samples per group, one-way ANOVA with Mann-Whitney test for mice and two-tailed Student's t-test for cell samples; *$p < 0.05$, **$p < 0.01$, ***$p < 0.001$.

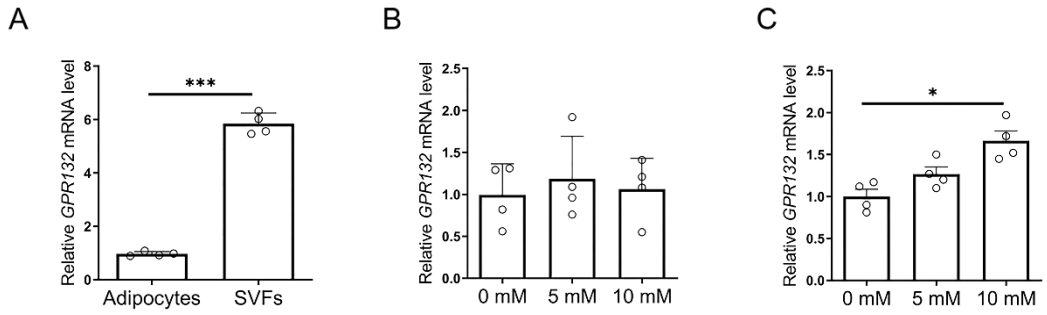

Figure S7. siRNA-mediated knockdown of GPR132 in BMDMs. BMDMs were transfected with a negative control siRNA or a siRNA targeting GPR132 for 48 h and lysed for immunoblots. Immunoblots for GPR132 in BMDMs and quantification of GPR132 to β-actin. Data are presented as means ± SD of 4 parallel samples per group, two-tailed Student's t-test; *$p < 0.05$, **$p < 0.01$, ***$p < 0.001$.

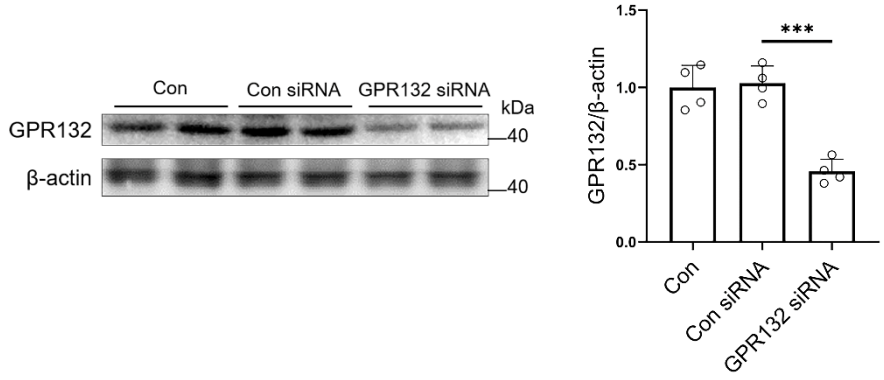

Figure S8. GPR132-PKA participated in the inhibition of L-lactate on macrophage M1 polarization. BMDMs were treated with vehicle, L-lactate, Con siRNA, or GPR132 siRNA, and then LPS was added. **A-B** Flow cytometry analyses of M1 surface marker CD38 **(A)** and CD274 **(B)**. **C** The mRNA levels of pro-inflammatory genes. In another independent study, BMDMs were treated with vehicle or L-lactate, and then LPS was added. H89 was used as a PKA inhibitor. **D-E** Flow cytometry analyses of M1 surface marker CD38 **(D)** and CD274 **(E)**. **F** The mRNA levels of pro-inflammatory genes. Data are presented as means ± SD of 4 parallel samples per group, two-tailed Student's t-test; *$p < 0.05$, **$p < 0.01$, ***$p < 0.001$. Lac, L-lactate.

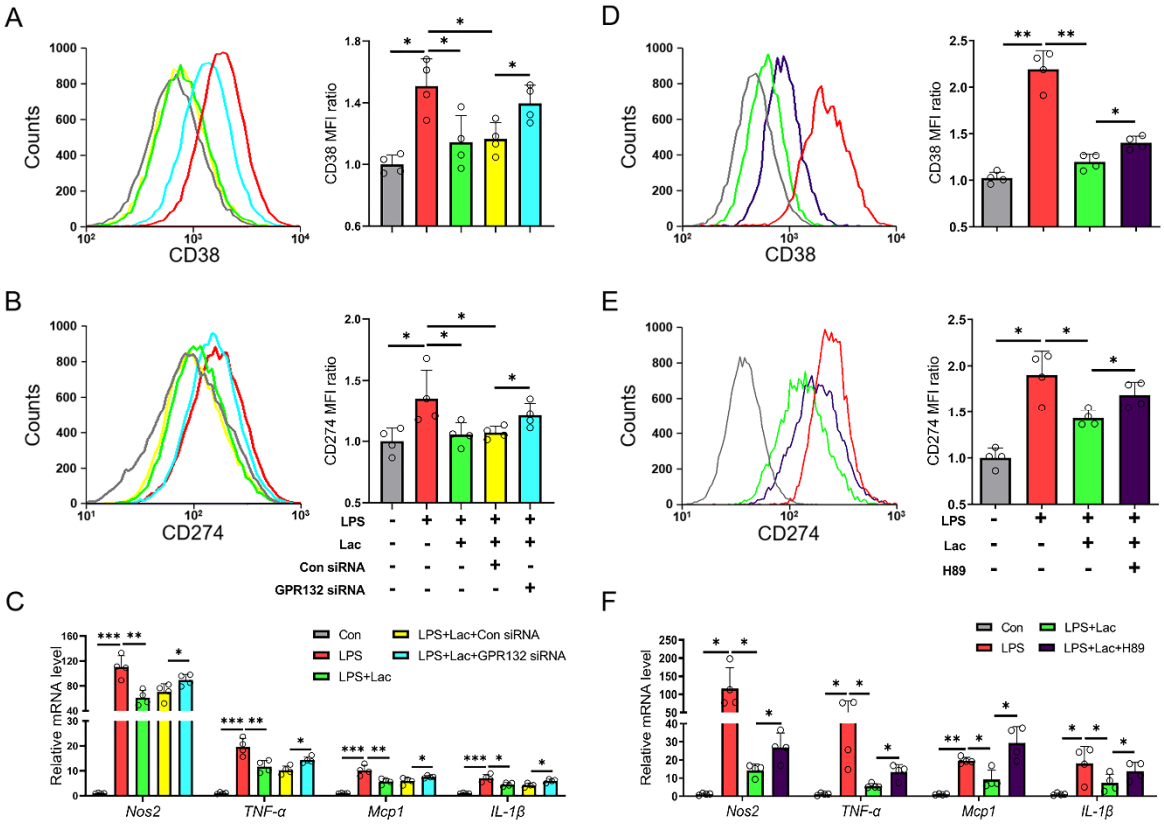

Figure S9. The expression of TGF-β1 and TGF-β2 in EATs. The 6-week-old male mice were divided into four groups, including LS, LL, HS, and HL groups. **A-B** The mRNA levels of *TGF-β1* **(A)** and *TGF-β2* **(B)**. **C** Immunoblots for TGF-β1 and TGF-β2 in EATs and quantification of TGF-β1 and TGF-β2 to β-actin. Data are presented as means ± SD of 8 mice per group, one-way ANOVA with Mann-Whitney test; *$p < 0.05$, **$p < 0.01$, ***$p < 0.001$. LS, LFD-saline (i.p.); LL, LFD-lactate (i.p.); HS, HFD-saline (i.p.); HL, HFD-lactate (i.p.).

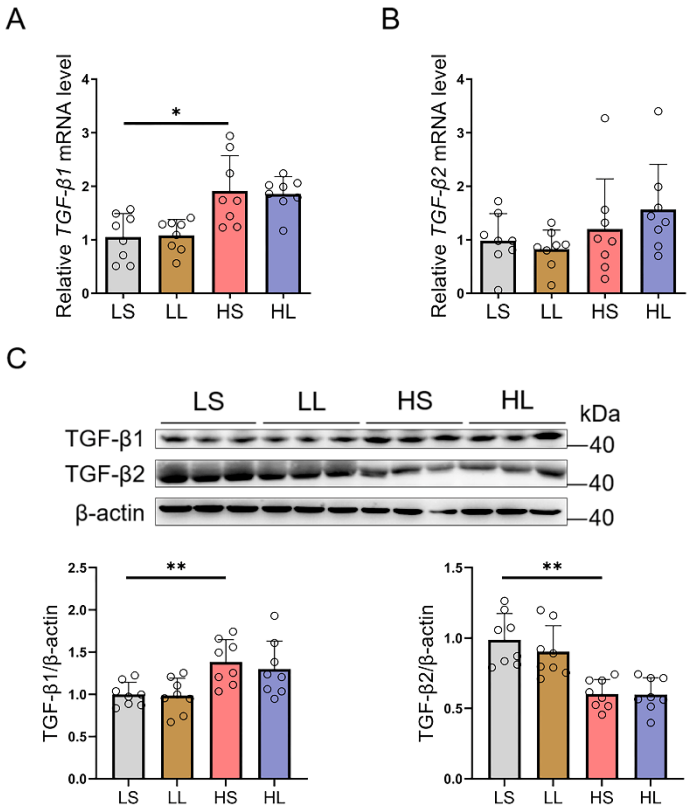

Figure S10. The proposed mechanism for moderate L-lactate administration improves adipose tissue insulin resistance. On the one hand, moderate L-lactate administration elevates adipose tissue mitochondrial thermogenic protein UCP1 expression. On the other hand, L-lactate could bind to the GPR132 on the membrane of macrophages and activates the downstream PKA-LKB1-AMPKα1 signal, which subsequently inhibits the NF-kB signal and the secretion of inflammatory cytokines. The suppression of moderate L-lactate administration on macrophage pro-inflammatory M1 polarization further promotes AKT phosphorylation and GLUT4 translocation in adipocytes. Collectively, moderate L-lactate administration activates adipose tissue macrophage GPR132-PKA-AMPKα1 pathway to alleviate obesity-associated insulin resistance in mice.

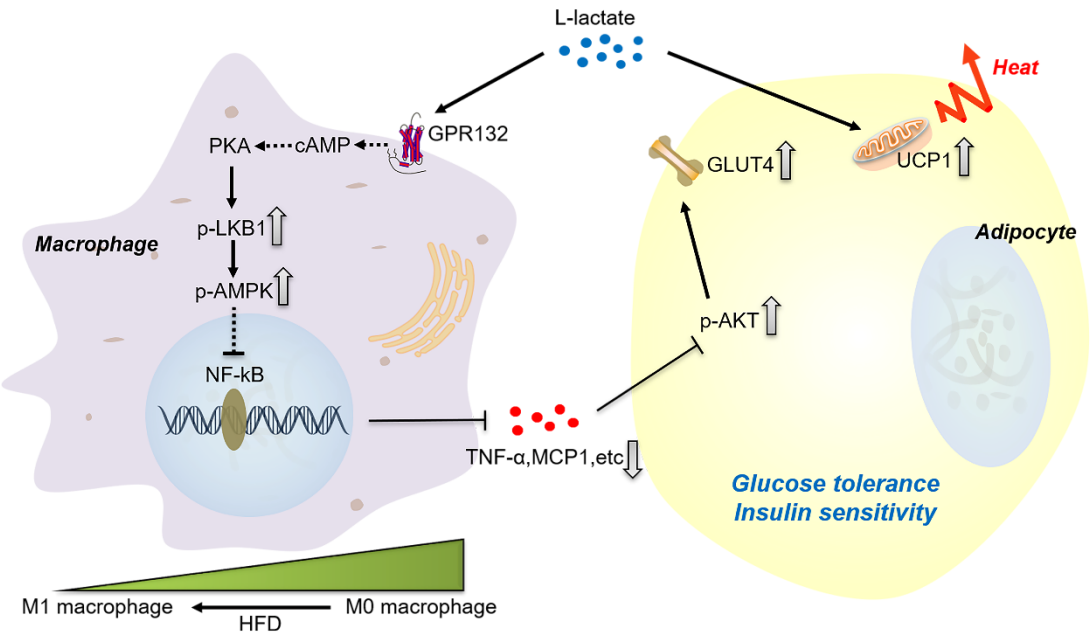

Table S1. The primer sequences used for qRT-PCR.

Gene	Forward primer	Reverse primer
β-actin	CATCCGTAAAGACCTCTATGCCAAC	ATGGAGCCACCGATCCACA
TNF-α	ACGGCATGGATCTCAAAGAC	AGATAGCAAATCGGCTGACG
IL-1β	CTTCCCCAGGGCATGTTAAG	ACCCTGAGCGACCTGTCTTG
IFN-γ	ATGAACGCTACACACTGCATC	CCATCCTTTTGCCAGTTCCTC
MCP1	CCCCAAGAAGGAATGGGTCC	GGTTGTGGAAAAGGTAGTGG
F4/80	TGACTCACCTTGTGGTCCTAA	CTTCCCAGAATCCAGTCTTTCC
Nos2	CCAAGCCCTCACCTACTTCC	CTCTGAGGGCTGACACAAGG
Arg1	CTCCAAGCCAAAGTCCTTAGAG	AGGAGCTGTCATTAGGGACATC
Ucp1	CACTCAGGATTGGCCTCTACG	GGGGTTTGATCCCATGCAGA
Prdm16	CCACCAGACTTCGAGCTACG	ACACCTCTGTATCCGTCAGCA
Pgc-1α	CCCTGCCATTGTTAAGACC	TGCTGCTGTTCCTGTTTTC
Cidea	TGACATTCATGGGATTGCAGAC	GGCCAGTTGTGATGACTAAGAC
GPR132	GTGCCATTGTGGATCATCTACA	CTCTCCAGTGCATAGACCACG
MCT1	TGTTAGTCGGAGCCTTCATTTC	CACTGGTCGTTGCACTGAATA
TGF-β1	CTCCCGTGGCTTCTAGTGC	GCCTTAGTTTGGACAGGATCTG
TGF-β2	CTTCGACGTGACAGACGCT	GCAGGGGCAGTGTAAACTTATT
Cpt1a	CTCCGCCTGAGCCATGAAG	CACCAGTGATGATGCCATTCT
Cpt2	CAGCACAGCATCGTACCCA	TCCCAATGCCGTTCTCAAAAT
Pkm2	GCCGCCTGGACATTGACTC	CCATGAGAGAAATTCAGCCGAG
G6pc	CGACTCGCTATCTCCAAGTGA	GTTGAACCAGTCTCCGACCA
CPT1b	GCACACCAGGCAGTAGCTTT	CAGGAGTTGATTCCAGACAGGTA
PPARα	AGAGCCCCATCTGTCCTCTC	ACTGGTAGTCTGCAAAACCAAA

Table S2. The antibodies used in this study.

	Antibody	Source	Catalog number	Dilution
Western blot	β-actin	Cell Signaling Technology	4967	5000
	AKT	Cell Signaling Technology	4691S	5000
	Phosphor-AKT	Cell Signaling Technology	9271S	1000
	AMPKα1	Cell Signaling Technology	2532S	1000
	Phosphor-AMPKα1	Cell Signaling Technology	2531S	1000
	LKB1	Cell Signaling Technology	3047	1000
	Phosphor-LKB1	Cell Signaling Technology	3482	1000
	UCP1	Abcam	ab209483	5000
	TGF-β1	Abcam	ab215715	1000
	TGF-β2	Abcam	ab36495	1000
	GPR132	Santa	sc-137112	200
	GLUT2	Proteintech	66889-1-Ig	5000
	GLUT4	Millipore	07-1404	1000
Flow cytometry	APC anti-mouse F4/80	BioLegend	123116	200
	FITC anti-mouse CD206	BioLegend	141704	300
	PE anti-mouse CD11c	eBioscience	12-0114	200
	APC anti-mouse CD274	BioLegend	124312	200
	PE anti-mouse CD38	BioLegend	102708	200